KARMEN: PRESENT NEUTRINO-OSCILLATION LIMITS AND PERSPECTIVES AFTER THE UPGRADE

KLAUS EITEL[a]
Forschungszentrum Karlsruhe, Institut für Kernphysik I
D-76021 Karlsruhe, Postfach 3640, Germany
E-mail: klaus@ik1.fzk.de

ABSTRACT

The neutrino experiment KARMEN is situated at the beam stop neutrino source ISIS. It provides ν_μ's, ν_e's and $\bar{\nu}_\mu$'s in equal intensities from the π^+–μ^+–decay at rest. The oscillation channels $\nu_\mu \rightarrow \nu_e$ and $\bar{\nu}_\mu \rightarrow \bar{\nu}_e$ are investigated with a 56 t liquid scintillation calorimeter at a mean distance of 17.6 m from the ν–source. No evidence for oscillations could be found with KARMEN, resulting in 90% CL exclusion limits of $sin^2(2\Theta) < 8.5 \cdot 10^{-3}$ $(\bar{\nu}_\mu \rightarrow \bar{\nu}_e)$ and $sin^2(2\Theta) < 4.0 \cdot 10^{-2}$ $(\nu_\mu \rightarrow \nu_e)$ for $\Delta m^2 > 100\,\mathrm{eV}^2$.
In 1996, the KARMEN neutrino experiment has been upgraded by an additional veto system. Vetoing of cosmic muons passing the 7000 t massive iron shielding of the detector suppresses energetic neutrons from deep inelastic scattering of muons as well as from μ–capture in iron. Up to 1996, these neutrons penetrating into the detector represented the main background for the $\bar{\nu}_\mu \rightarrow \bar{\nu}_e$ oscillation search. With an expected reduction of the background rate by a factor of 40 the experimental sensitivity for $\bar{\nu}_\mu \rightarrow \bar{\nu}_e$ will be significantly enhanced towards $sin^2(2\Theta) \approx 1 \cdot 10^{-3}$ for large Δm^2.

1. Neutrino Production at ISIS

The Karlsruhe Rutherford Medium Energy Neutrino experiment KARMEN is being performed at the neutron spallation facility ISIS of the Rutherford Appleton Laboratory. The neutrinos are produced by stopping 800 MeV protons in a beam dump Ta-D_2O-target. Neutrinos emerge from the consecutive decay sequence $\pi^+ \rightarrow \mu^+ + \nu_\mu$ and $\mu^+ \rightarrow e^+ + \nu_e + \bar{\nu}_\mu$.

[a]for the KARMEN Collaboration

Thus, ISIS represents a ν-source with identical intensities for ν_μ, ν_e and $\bar{\nu}_\mu$ emitted isotropically ($\Phi_\nu = 6.37 \cdot 10^{13}\,\nu$/s per flavor for p-beam current $I_p = 200\,\mu$A). The energy spectra of the ν's are well defined due to the decay at rest of both the π^+ and μ^+(fig. 1a). The ν_μ's from

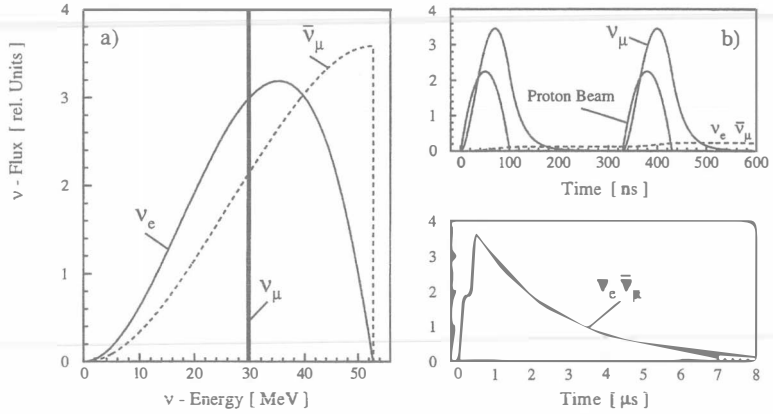

Fig. 1. Neutrino energy spectra (a) and production times (b) at ISIS.

π^+–decay are monoenergetic (E_ν=30 MeV), the continous energy distributions of ν_e and $\bar{\nu}_\mu$ up to 52.8 MeV can be calculated using the V–A theory. Since π^+ and μ^+ are stopped in the small beam dump target, the ν production region is essentially limited to a volume of $\pm$5 cm radial to the proton beam and $\pm$10 cm along the beam axis. With a mean distance source–detector of $L = 17.6$ m and including the spatial resolution of the detector, the uncertainty $\Delta L/L$ for the ν flight path is less than 1%. ISIS therefore ensures that the important experimental parameters L and E_ν for ν–oscillations are determined with high precision.

Two parabolic proton pulses of 100 ns basis width and a gap of 225 ns are produced with a repetition frequency of 50 Hz (fig. 1b). The different lifetimes of pions ($\tau = 26$ ns) and muons ($\tau = 2.2\,\mu$s) allow a clear separation in time of the ν_μ-burst from the following ν_e's and $\bar{\nu}_\mu$'s. Furthermore the accelerator duty cycle allows effective suppression of any beam-uncorrelated background by four to five orders of magnitude.

2. The KARMEN Detector

The neutrinos are detected in a 56 t liquid scintillation calorimeter [1]. A massive blockhouse of 7000 t of steel in combination with a system of two layers of active veto counters provides shielding against beam correlated spallation neutron background, suppression of the hadronic component of cosmic radiation as well as reduction of the flux of cosmic muons. The central scintillation calorimeter and the inner veto counters are segmented by double acrylic walls with an air gap allowing efficient light transport via total internal reflection of the scintillation light at the module walls. The event position is determined by the individual module and the time difference of the PM signals at each end of this module. Due to the optimized optical properties of the organic liquid scintillator and an active volume of 96% for the calorimeter, an excellent energy resolution of $\sigma_E = \frac{11.5\%}{\sqrt{E[MeV]}}$ is achieved. In addition, Gd_2O_3 coated paper within the module walls provides efficient detection of thermal neutrons due to the very high capture

cross section of the Gd(n,γ) reaction. The KARMEN electronics is synchronized to the ISIS proton pulses to an accuracy of better than ± 2 ns, so that the time structure of the neutrinos, especially of ν_μ's, can be exploited in full detail. In these proceedings we only present results of the oscillation search and its results obtained in the first data taking period from 1990–1995, the investigation of ν–nucleus interactions on ^{12}C is described elsewhere[2] in detail.

3. Oscillation limits on $\nu_\mu \rightarrow \nu_e$

In the event of $\nu_\mu \rightarrow \nu_e$ oscillations, monoenergetic 30 MeV ν_e's would arise in the ν_μ time window after beam-on-target. The ν_e detection reaction is $^{12}\mathrm{C}(\nu_e, \mathrm{e}^-)^{12}\mathrm{N}_{\mathrm{g.s.}}$ followed by the β–decay $^{12}\mathrm{N}_{\mathrm{g.s.}} \rightarrow {}^{12}\mathrm{C} + \mathrm{e}^+ + \nu_e$. One would therefore expect electrons with a peaked energy spectrum ($E_{e^-} = E_\nu - Q = 29.8 - 17.3 = 12.5$ MeV, see fig. 2a) within the two ν_μ time pulses (fig. 2b). This characteristic prompt energy signal is followed by the energy of the sequential spatially correlated e^+ (fig. 2c) which follows the e^- with the typical ^{12}N decay time (fig. 2d). In

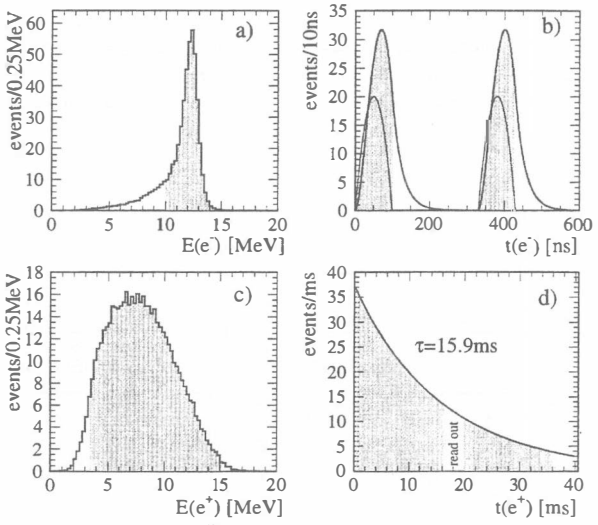

Fig. 2. Expected signature for $\nu_\mu \rightarrow \nu_e$ full oscillation:
a) simulated MC energy of prompt event; b) proton pulses and time of prompt event relative to ISIS beam-on-target; c) MC energy of sequential event; d) time difference between prompt and sequential event; shaded areas show the allowed regions of evaluation cuts.

the later ν_μ time window one can measure the number of $^{12}\mathrm{C}(\nu_e, \mathrm{e}^-)^{12}\mathrm{N}_{\mathrm{g.s.}}$ reactions induced by ν_e's from μ^+-decay in the ISIS target, which can be used to calculate the expectation of $\nu_\mu \rightarrow \nu_e$ induced CC reactions for $P_{\nu_\mu \rightarrow \nu_e} = 100\%$. The different detection efficiencies and the energy dependence of the cross section have to be taken into account to extract the ν-flux and cross section independent expectation of 187.8 oscillation signatures. Applying all cuts (e.g. $10 \leq E_{pr} \leq 14$ MeV; $0 \leq t_{pr} \leq 100$ns or $325 \leq t_{pr} \leq 425$ns) only 2 sequences remain within the data taken between July 1992 and December 1995. 0.50 ± 0.20 cosmic induced events contribute to the background which is dominated by the small contribution of ν_e's from μ^+–decay within the two 100 ns long ν_μ–time intervals after beam-on-target (1.76 ± 0.2). With a total background of $N_{bg} = 2.26 \pm 0.3$ events, there is no hint for $\nu_\mu \rightarrow \nu_e$ oscillations and an upper

limit of the oscillation probability P of

$$P_{\nu_\mu \to \nu_e} < 3.8/187.8 = 2.0 \cdot 10^{-2} \qquad (90\%\, CL)$$

can be extracted. Due to the normalization of the full oscillation expectation this result is very reliable. The oscillation search is nearly background free so that the sensitivity for this oscillation channel is essentially limited by the relatively small expectation value for full oscillation, i.e. statistics.

4. Oscillation limits on $\bar{\nu}_\mu \to \bar{\nu}_e$

The most sensitive mode of the KARMEN experiment for the search of ν-oscillations is the $\bar{\nu}_\mu \to \bar{\nu}_e$ channel. First, $\bar{\nu}_e$'s are not produced within the ISIS target apart from a very small contamination of $\bar{\nu}_e/\nu_e < 6 \cdot 10^{-4}$. The detection of $\bar{\nu}_e$'s via $\mathrm{p}(\bar{\nu}_e, \mathrm{e}^+)\mathrm{n}$ would therefore indicate oscillations $\bar{\nu}_\mu \to \bar{\nu}_e$ in the appearance channel. Secondly, the cross section for $\mathrm{p}(\bar{\nu}_e, \mathrm{e}^+)\mathrm{n}$ with $\bar{\nu}_e$'s from oscillations ($\sigma = 93.6 \cdot 10^{-42}\mathrm{cm}^2$ for $\Delta m^2 = 100\,\mathrm{eV}^2$) is about 20 times larger than for $^{12}\mathrm{C}(\nu_e, \mathrm{e}^-)^{12}\mathrm{N}_{\mathrm{g.s.}}$ with ν_e's from $\nu_\mu \to \nu_e$ ($\sigma = 4.95 \cdot 10^{-42}\mathrm{cm}^2$), and the ratio of target nuclei of the scintillator is $H/C = 1.767$.

The signature for the detection of $\bar{\nu}_e$'s is a spatially correlated delayed coincidence of positrons from $\mathrm{p}(\bar{\nu}_e, \mathrm{e}^+)\mathrm{n}$ with energies up to $E_{e^+} = E_{\bar{\nu}_e} - Q = 52.8 - 1.8 = 51\,\mathrm{MeV}$ (fig. 3a) and γ emission of either of the two neutron capture processes $\mathrm{p}(\mathrm{n},\gamma)\mathrm{d}$ or $\mathrm{Gd}(\mathrm{n},\gamma)\mathrm{Gd}$ with γ energies of 2.2 MeV or up to 8 MeV, respectively (fig. 3b). The positrons are expected in a time

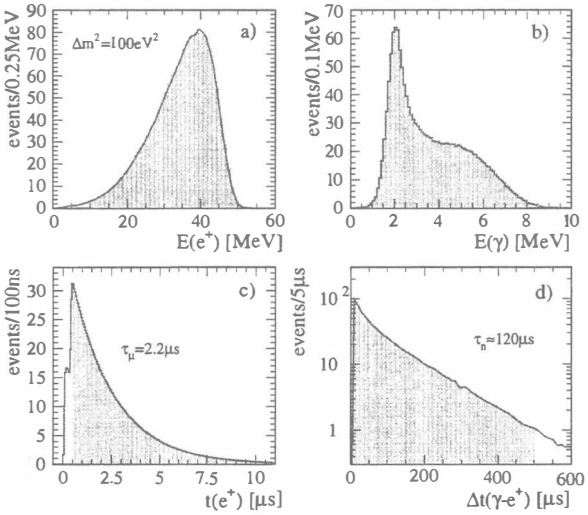

Fig. 3. Expected signature for $\bar{\nu}_\mu \to \bar{\nu}_e$ full oscillation:
a) MC energy of prompt positron for $\Delta m^2 = 100\mathrm{eV}^2$; b) energy of sequential γ's; c) time of prompt event relative to ISIS beam-on-target; d) time difference between prompt e^+ and sequential γ's; shaded areas are accepted by evaluation cuts.

window of 0.5 to 10.5 μs after beam-on-target (fig. 3c). The neutrons from $\mathrm{p}(\bar{\nu}_e, \mathrm{e}^+)\mathrm{n}$ are thermalized and captured typically with $\tau = 120\,\mu\mathrm{s}$ (fig. 3d). The neutron detection efficiency for the analyzed data is 28.2%. The data set remaining after applying all cuts in energy, time and spatial correlation is shown in fig. 4. A prebeam analysis of cosmic ray induced sequences

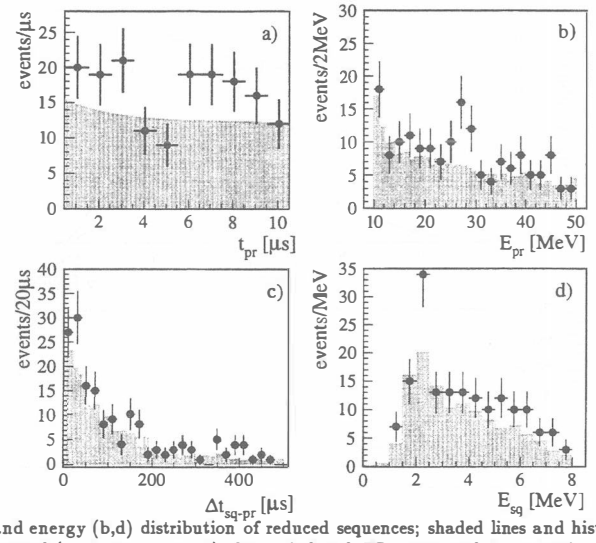

Fig. 4. Time (a,c) and energy (b,d) distribution of reduced sequences; shaded lines and histograms represent the pre-beam background (12.2 events per μs) plus ν_e-induced CC events and $\bar{\nu}_e$-contamination.

results in an accumulated background level of 12.2 ± 0.2 events per μs in the prompt 10 μs–window (see fig. 4a). The actual rate is $16.4 \pm 1.3/\mu$s which corresponds to a beam excess of 2.4 σ compared with the prebeam level including ν_e-induced CC (9 events) and $\bar{\nu}_e$-contamination (1.7 events). Although the secondary part of the sequences shows the typical signature of thermal neutron capture, the prompt time and energy distribution does not follow the expectation from $\bar{\nu}_\mu \rightarrow \bar{\nu}_e$ oscillation with $\Delta m^2 = 100\,\mathrm{eV}^2$.

To extract a possible small contribution of $\bar{\nu}_\mu \rightarrow \bar{\nu}_e$, the data set is scanned with a two-dimensional maximum likelihood analysis on time and energy distribution of the positrons requiring a 2.2 μs exponential time constant for the e^+ and a time independent cosmic induced background. The measurement of the e^+ energy with spectroscopic quality is highly sensitive to changes in the energy spectrum due to the dependence of the oscillation probability on the mass term Δm^2 (see fig. 5a). The energy distributions of the positrons used in the likelihood analysis therefore have been tested with spectra for Δm^2 in the range from 0.01 to $100\,\mathrm{eV}^2$.

For most of the investigated parameter range of Δm^2 the likelihood analysis results in best fit values compatible with a zero signal within a 1σ error band (see fig. 5b). Only for a parameter region at $\Delta m^2 = 6.2\,\mathrm{eV}^2$ there is a positive signal 2.3σ above zero which is not considered as statistically significant. In addition, this Δm^2-value corresponds to the first theoretical oscillation minimum in the detector with the lowest possible mean energy of the positrons (see also fig. 5a) and represents therefore an extremum in the likelihood analysis which should be interpreted with special precaution.

On this basis of no evidence for oscillations, 90% CL upper limits for oscillation events (fig. 5b) as well as for the oscillation parameters Δm^2 and $sin^2(2\Theta)$ are deduced. Our result can be compared with an expected signal of 6 up to 76 events for $\Delta m^2 = 3.9\,\mathrm{eV}^2$ based on a recently published oscillation probability of $P_{\bar{\nu}_\mu \rightarrow \bar{\nu}_e} = 0.0031$ by LSND [3]. For large Δm^2 we expect at KARMEN 1898 detected oscillation events for full oscillation which results in an upper limit of the mixing angle

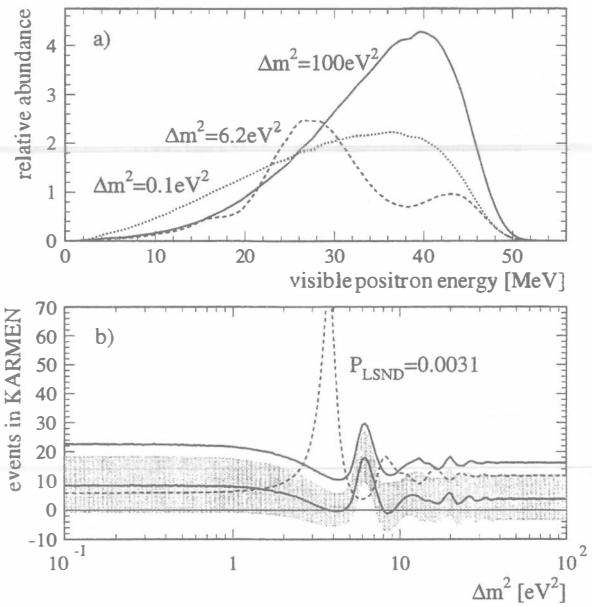

Fig. 5. a) Examples of expected e^+–spectra (visible energy including detector response) for different oscillation parameters Δm^2; b) likelihood-fit results depending on Δm^2; the shaded area represents the 1σ-error band around the best fit values for $\Delta m^2 = 0.01 \ldots 100\,\mathrm{eV}^2$; the solid line above the shaded band shows the 90% CL upper limit from KARMEN, the broken line the expected event numbers in KARMEN based on the LSND oscillation evidence [3].

$$sin^2(2\Theta) < 16.3/1898 = 8.5 \cdot 10^{-3} \quad \text{for large } \Delta m^2 \qquad (90\%\, CL\ ).$$

Fig. 6 shows the KARMEN exclusion curves in the parameter space of Δm^2 and $sin^2(2\Theta)$ in a two neutrino flavor oscillation calculation for the appearance channels $\nu_\mu \rightarrow \nu_e$ and $\bar{\nu}_\mu \rightarrow \bar{\nu}_e$ in comparison with other results of ν–oscillation searches at accelerators [4] and reactors [5]. As the sensitivity for $\bar{\nu}_\mu \rightarrow \bar{\nu}_e$ of the KARMEN experiment is comparable to that of LSND (both experiments expect about 2000 oscillation events for $\Delta m^2 > 100\,\mathrm{eV}^2$ and $sin^2(2\Theta) = 1$ on their data sample until 1995), the KARMEN 90% CL exclusion curve cannot exclude the entire parameter space favoured by the positive result of LSND.

5. The KARMEN Upgrade

For at least the next 3 years, no other oscillation experiment will cover the whole parameter region favored by LSND. Only the running KARMEN experiment, with an improved sensitivity, will be able to crosscheck the evidence postulated by LSND. We therefore investigated different scenarios for increasing the $\bar{\nu}_\mu \rightarrow \bar{\nu}_e$ sensitivity. Whereas the sensitivity for $\nu_\mu \rightarrow \nu_e$ oscillations is essentially limited by statistics, the KARMEN sensitivity in the $\bar{\nu}_\mu \rightarrow \bar{\nu}_e$ channel can only be substantially increased by the reduction of the small but dominant cosmogenic background (see fig. 4). This background is induced by cosmic muons stopping or undergoing deep inelastic scattering in the iron shielding which surrounds the KARMEN detector and veto system. Energetic neutrons emitted in these processes can penetrate deep into the detector without

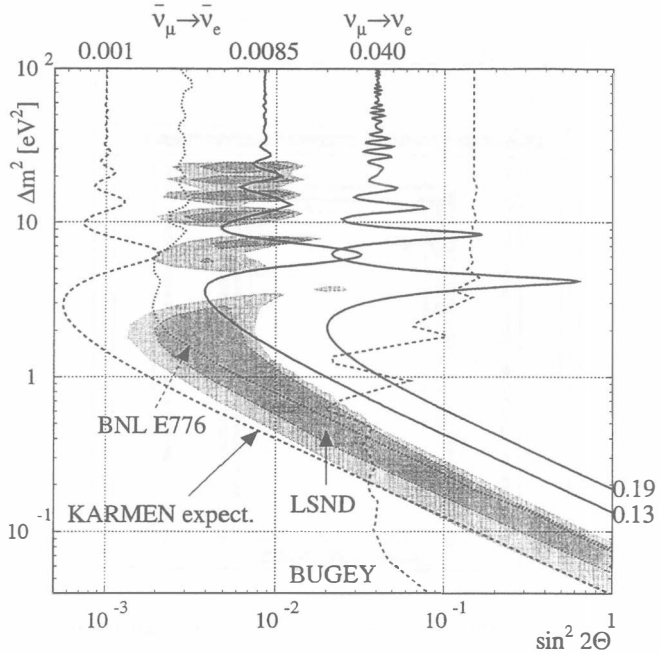

Fig. 6. 90% CL exclusion curves and limits for $\Delta m^2 = 100\,\mathrm{eV}^2$, $sin^2(2\Theta) = 1$ from KARMEN for $\nu_\mu \rightarrow \nu_e$ and $\bar{\nu}_\mu \rightarrow \bar{\nu}_e$ as well as the expected sensitivity for $\bar{\nu}_\mu \rightarrow \bar{\nu}_e$ after the upgrade; oscillation limits from BNL E776 [4] and Bugey [5]; LSND evidence is shown as shaded areas (90% CL and 99% CL areas respectively).

triggering the veto system, thus producing an event sequence of prompt recoil protons followed by the capture of the then thermalized neutrons.

To tag the original muons in the vicinity of the detector, a further active veto layer within the blockhouse has been built in 1996, which consists of 136 plastic scintillator bars (BICRON BC 412) of lengths up to 4 m, 65 cm width and 5 cm thickness, with a total surface of 300 m^2 covering all sides of the detector (fig. 7). There is at least 1 m between the new counter and the existing shield so that energetic neutrons produced by cosmic muons outside the new veto system have to travel a path of more than 4 attenuation lengths in iron ($\Lambda = 21$ cm). This reduces cosmogenic neutrons to a negligible fraction of less than 1.5% of the original flux. The new veto system is designed to reduce cosmogenic sequential background by a factor of at least 40. This reduction factor is based on detailed background measurements and extensive GEANT MC simulations of cosmic muons. First preliminary evaluations of cosmic background in a prebeam window indicate the expected reduction factor in the energy region of interest when the information of veto hits is included in the analysis.

After two years of measuring time with the new detector configuration, the KARMEN sensitivity for $\bar{\nu}_\mu \rightarrow \bar{\nu}_e$ is expected to exclude the whole parameter region of evidence suggested by LSND if no oscillation signal will be found (fig. 6). In that case, mixing angles with $sin^2(2\Theta) > 1 \cdot 10^{-3}$ will be excluded for large Δm^2. The veto upgrade will also increase the signal to background ratio of single prong ν-induced events on ^{12}C and therefore improve the

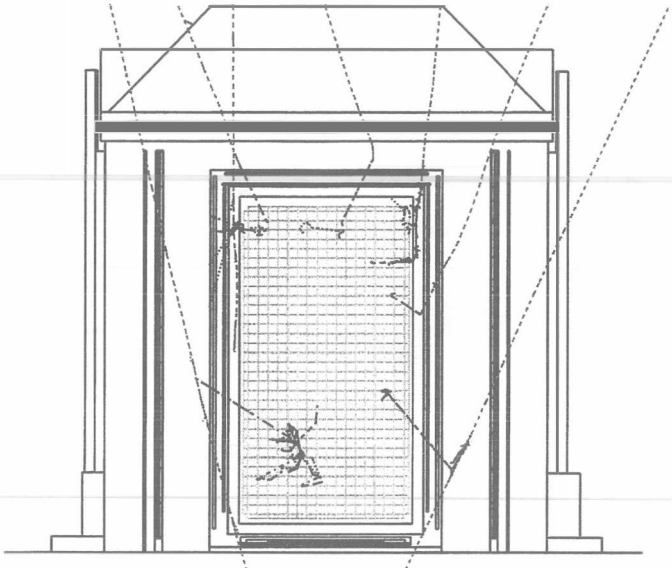

Fig. 7. Cross section of the KARMEN central detector with surrounding shield counters and massive iron blockhouse, now including the additional veto system. Cosmic muons passing or stopping in the iron which produce energetic neutrons can now be tagged by the new veto scintillators.

investigation of the published anomaly in this time distribution [6].

6. Acknowledgements

We acknowledge the financial support of the German Bundesministerium für Bildung, Wissenschaft, Forschung und Technologie.

7. References

1) G. Drexlin et al., *Nucl. Instr. and Meth.* **A289** (1990) 490.
2) B. A. Bodmann et al., *Phys. Lett.* **B339** (1994) 215.
B. Zeitnitz et al.,*Prog. Part. Nucl. Phys.* **32** (1994) 351.
3) C. Athanassopoulos et al., *Phys. Rev. C* **54** (1996) 2685.
C. Athanassopoulos et al., *Phys. Rev. Letters* **77** (1996) 3082.
4) L. Borodovsky et al., *Phys. Rev. Letters* **68** (1992) 274.
5) B. Achkar et al., *Nucl. Phys.* **B434** (1995) 503.
6) B. Armbruster et al., *Phys. Lett.* **B348** (1995) 19.